Factors Influencing Optical Coherence Tomography Peripapillary Choroidal Thickness: A Multicenter Study

Hongli Yang,[1] Haomin Luo,[1,2] Stuart K. Gardiner,[3] Christy Hardin,[1] Glen P. Sharpe,[4] Joseph Caprioli,[5] Shaban Demirel,[3] Christopher A. Girkin,[6] Jeffrey M. Liebmann,[7] Christian Y. Mardin,[8] Harry A. Quigley,[9] Alexander F. Scheuerle,[10] Brad Fortune,[3] Balwantray C. Chauhan,[4] and Claude F. Burgoyne[1]

[1]Devers Eye Institute, Optic Nerve Head Research Laboratory, Legacy Research Institute, Portland, Oregon, United States
[2]Department of Ophthalmology, Second Xiangya Hospital, Central South University, Changsha, Hunan Province, People's Republic of China
[3]Devers Eye Institute, Discoveries in Sight Research Laboratories, Legacy Research Institute, Portland, Oregon, United States
[4]Ophthalmology and Visual Sciences, Dalhousie University, Halifax, Nova Scotia, Canada
[5]Jules Stein Eye Institute, David Geffen School of Medicine at University of California at Los Angeles, Los Angeles, California, United States
[6]Department of Ophthalmology, School of Medicine, University of Alabama at Birmingham, Birmingham, Alabama, United States
[7]Einhorn Clinical Research Center, Moise and Chella Safra Advanced Ocular Imaging Laboratory, New York Eye and Ear Infirmary of Mount Sinai Health System, New York, United States
[8]Department of Ophthalmology, University of Erlangen, Erlangen, Germany
[9]Wilmer Eye Institute, Johns Hopkins University, Baltimore, Maryland, United States
[10]Department of Ophthalmology, University of Heidelberg, Heidelberg, Germany

Correspondence: Claude F. Burgoyne, Optic Nerve Head Research Laboratory, Devers Eye Institute, Legacy Research Institute, 1225 NE 2nd Avenue, Portland, OR 97208-3950, USA; cfburgoyne@deverseye.org.

HY and HL contributed equally to the work presented here and should therefore be regarded as equivalent authors.

Submitted: July 30, 2018
Accepted: November 25, 2018

Citation: Yang H, Luo H, Gardiner SK, et al. Factors influencing optical coherence tomography peripapillary choroidal thickness: a multi-center study. *Invest Ophthalmol Vis Sci*. 2019;60:795–806. https://doi.org/10.1167/iovs.18-25407

Purpose. To quantify peripapillary choroidal thickness (PCT) and the factors that influence it in healthy participants who represent the racial and ethnic composition of the U.S. population.

Methods. A total of 362 healthy participants underwent optical coherence tomography (OCT) enhanced depth imaging of the optic nerve head with a 24 radial B-scan pattern aligned to the fovea to Bruch's membrane opening axis. Bruch's membrane, anterior scleral canal opening (ASCO), and the anterior scleral surface were manually segmented. PCT was measured at 100, 300, 500, 700, 900, and 1100 μm from the ASCO globally and within 12 clock-hour sectors. The effects of age, axial length, intraocular pressure, ethnicity, sex, sector, and ASCO area on PCT were assessed by ANOVA and univariable and multivariable regressions.

Results. Globally, PCT was thicker further from the ASCO border and thinner with older age, longer axial length, larger ASCO area, European descent, and female sex. Among these effectors, age and axial length explained the greatest proportion of variance. The rate of age-related decline increased further from the ASCO border. Sectorally, the inferior-temporal sectors were thinnest (10.7%–20.0% thinner than the thickest sector) and demonstrated a higher rate of age-related loss (from 15.6% to 20.7% faster) at each ASCO distance.

Conclusions. In healthy eyes, PCT was thinnest in the inferior temporal sectors and thinner PCT was associated with older age, European descent, longer axial length, larger ASCO area, and female sex. Among these associations, age had the strongest influence, and its effect was greatest within the inferior temporal sectors.

Keywords: peripapillary choroid, glaucoma, optic nerve head, 3D imaging, optical coherence tomography, peripapillary atrophy, imaging anatomy

Optical coherence tomography (OCT) permits the visualization and segmentation of Bruch's membrane, Bruch's membrane opening (BMO), the anterior scleral surface, the neural canal boundary, and the anterior scleral canal opening (ASCO; Figs. 1, 2).[1] Using these OCT landmarks to measure peripapillary choroidal thickness (PCT) enables both its cross-sectional characterization in healthy and diseased eyes and the longitudinal detection of PCT change in the locations that give rise to peripapillary atrophy (Fig. 3). The contribution of PCT and its change over time to the detection of glaucoma and other progressive conditions such as degenerative myopia can thus be assessed.

Alteration to the tissues of the peripapillary sclera, posterior ciliary arteries, choroid, and retina are thought to underlie the various clinical presentations of peripapillary atrophy in aging, glaucoma, and myopia.[2–8] Hayreh[9] and others[10,11] have hypothesized that peripapillary atrophy in glaucoma is a manifestation of compromised peripapillary choroidal blood flow within the posterior ciliary artery branches that penetrated the sclera immediately adjacent to the ASCO (hereafter

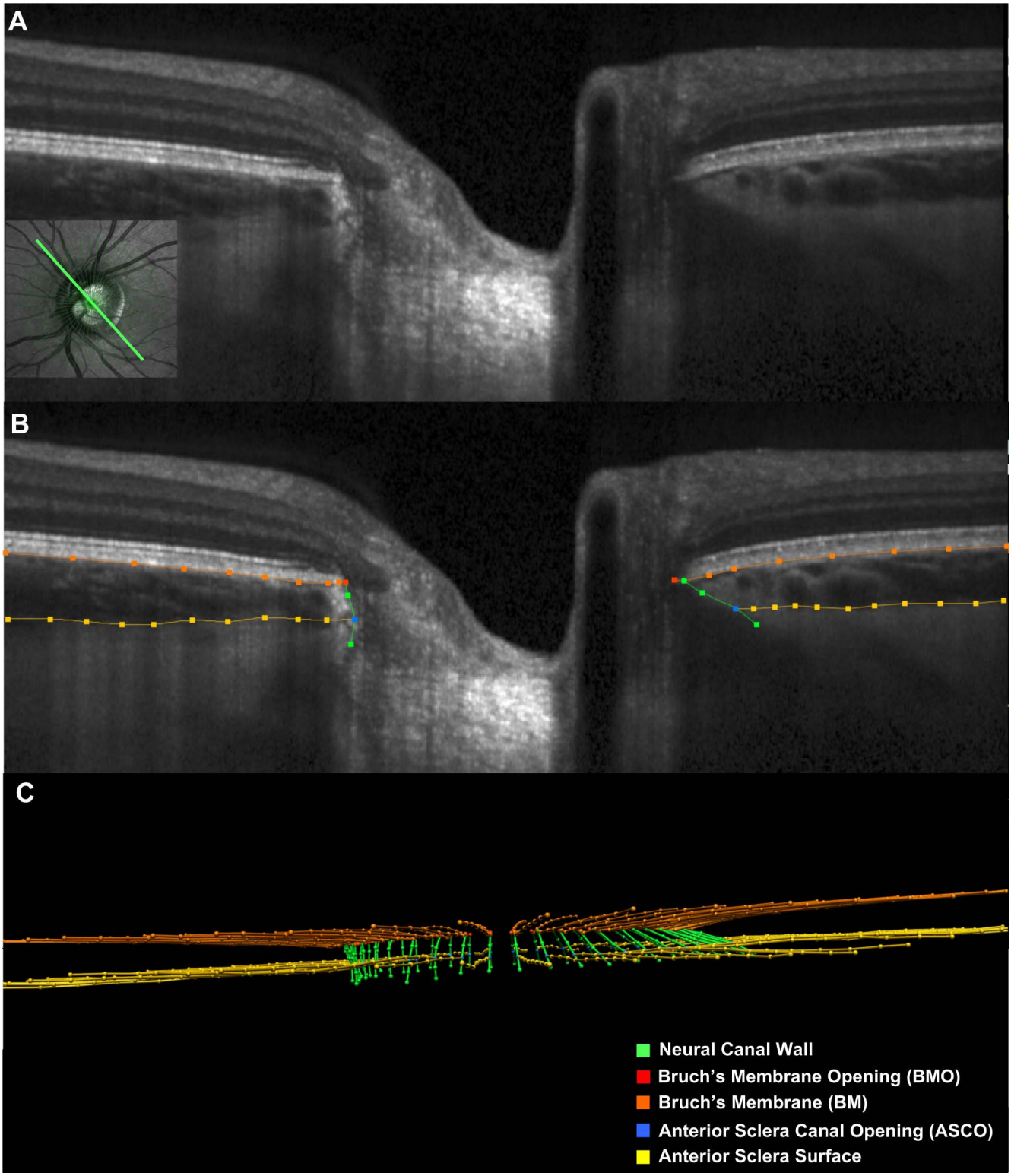

Figure 1. Manual segmentation of each radial B-scan. (**A**) A representative 15^{0} radial B-scan is shown with its location depicted in *green* within the inlayed infrared reflectance (IR) image (*bottom left*). (**B**) Manually segmented ONH landmarks for this study within the B-scan shown in (**A**). O*range lines/points* are the posterior surface of the Bruch's Membrane/RPE complex, *gold lines/points* are the anterior surface of the sclera. *Green lines/points* are the neural canal wall, *red points* are BMO, and *blue points* are the ASCO. (**C**) Point cloud of segmented points from the complete set of 24 radial B-scans obtained for this ONH.

Investigative Ophthalmology & Visual Science

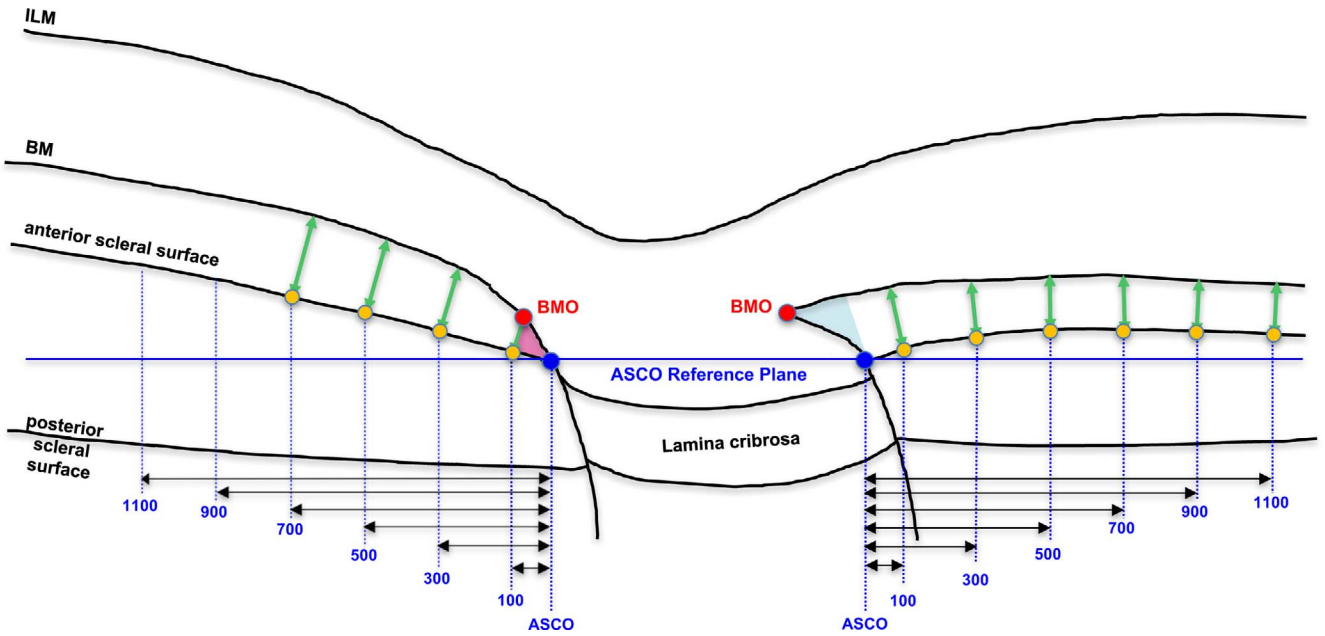

Figure 2. Measurement of peripapillary choroidal thickness at six distances (measured in microns) from the ASCO within the ASCO reference plane. Within the three-dimensional point cloud of segmented points from each OCT ONH data set (Figure 1C, above), Bruch's membrane and anterior scleral surface points were interpolated using b-splines. PCT was assessed in microns at six distances (*vertical blue dotted lines*) from the ASCO, measured within the ASCO reference plane (*horizontal blue line*). Each measurement distance was projected from the ASCO to the anterior sclera surface (*yellow dots*). At each anterior scleral measurement point, PCT was defined by the minimum distance to the posterior surface of Bruch's membrane (*green arrows*: PCT-100, PCT-300, PCT-500, PCT-700, PCT-900, and PCT-1100, respectively). In this study, PCT measurements within the regions of border tissues of Elschnig (BTE) obliqueness (*pink* externally oblique, *left*; *blue* internally oblique, *right*) were not included in the normative values as explained in Figure 3.

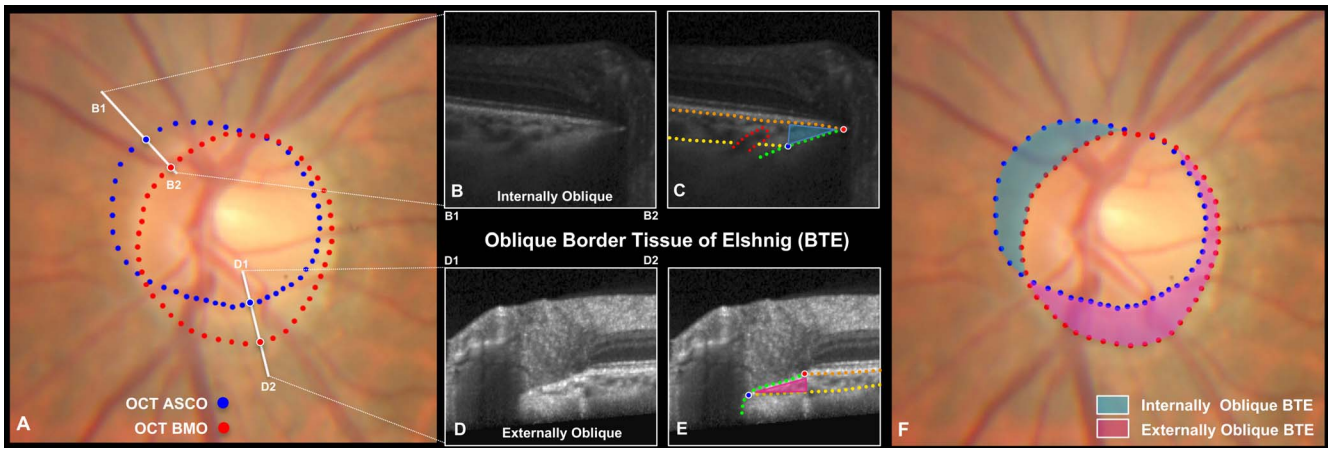

Figure 3. Although regions of internally and externally oblique BTE are defined by the offset of OCT BMO relative to OCT ASCO, PCT measurements within these regions are not included in the normative values of this report. (**A**) Color optic disc photo of the study eye of subject FDA287, with colocalized OCT ASCO (*blue*) and OCT BMO (*red*) points. The location and orientation (B1–B2) and (D1-D2) of the cropped B-scans shown in **B, C** and **D, E** are shown. (**B**) Cropped superior-nasal B-scan in a region of internally oblique BTE, (B1-B2) shown in **A** and delineated in (**C**). Note that BMO is "internal" to ASCO (or closer to the center of the disc). Note also that the suggestion of a juxta-scleral canal posterior ciliary vessel entering the choroid from the sclera (*red dots*). (**D**) Cropped *inferior-temporal* B-scan in a region of externally oblique BTE (D1-D2) shown in **A** and delineated in (**E**). Note that BMO is "external" to ASCO (or farther from the center of the disc). Although externally oblique border tissues do not represent atrophy in any form, they are commonly referred to as gamma peripapillary atrophy in the clinical[55] and OCT[4,56,57] literature. (**F**) The clinical extent of internally (*blue*) and externally (*pink*) oblique BTE in a healthy study eye with mild myopia (spherical equivalent –4.25D, axial length 25.13 mm). In this cross-sectional study, PCT measurements within the regions of BTE obliqueness were not included in the normative values because when present the density of the border tissues themselves and the adjacent choroidal septa made the presence of active choroidal vasculature difficult to determine and because the occurrence and regional distribution of internally and externally oblique border tissues are not consistent among all human eyes.[20] However, PCT can be measured relative to the ASCO within both forms of oblique border tissue regions, and the individual eye longitudinal change within these regions may be clinically important.

referred to as the juxta-scleral canal posterior ciliary artery branches; Fig. 3).[9,12] These branches are important because they also supply the circle of Zinn-Haller,[9,13,14] the laminar beam capillaries, and the retrolaminar orbital optic nerve and may thus separately contribute to the optic nerve head (ONH) pathophysiology of aging, glaucoma, and myopia.[2,12]

As a first step toward using OCT measurements of PCT in the detection of glaucoma or pathological myopia and their progression, the purpose of the present study was to measure PCT in a large group of healthy eyes relative to the ASCO at six proximal to distal measurement locations (100 μm, 300 μm, 500 μm, 700 μm, 900 μm, and 1100 μm, respectively). A second purpose of this study was to report and compare the influence of age, axial length, ethnicity, sex, IOP, and ASCO area on peripapillary choroidal thickness at each measurement location both globally and by foveal-BMO (FoBMO) 30^0 sectors.[1]

The majority of studies in which PCT is measured by OCT employ BMO as the reference opening for its regional quantification and Bruch's membrane as the reference for the thickness measurement.[15–17] PCT is measured from Bruch's membrane to the anterior scleral surface at measurement points that are located at fixed distances along Bruch's membrane from BMO. In this study, PCT was assessed at six distances from the ASCO, measured within an ASCO reference plane. Each measurement location was projected to the anterior sclera surface from which a measurement to Bruch's membrane was made (Fig. 2). We chose this approach for four reasons. First, BMO can be difficult to distinguish within the temporal region of myopic eyes.[18] Second, segmenting both the ASCO and BMO in a given eye primarily identifies the location and extent of oblique border tissue regions (Fig. 3). Third, we believe that the ASCO and the anterior scleral surface will be more stable as anatomic landmarks than BMO and Bruch's membrane[1,16] during the course of peripapillary choroidal thinning in aging, glaucoma, and myopia. Fourth, measurement locations within an ASCO reference plane should be less influenced by disease-related distortions in the ASCO or anterior scleral canal surface.[1,16,19]

In the present cross-sectional study, we do not include PCT measurements within oblique border tissue regions because the density of the border tissues themselves and the adjacent choroidal septa make the presence of active choroidal vasculature difficult to determine (Fig. 3) and because the regional distribution and extent of internally and externally oblique border tissues are not consistent among human eyes.[20] However, we predict that oblique border tissue regions will be most susceptible to longitudinal PCT thinning because PCT is the thinnest in these regions (Fig. 3). We further predict that longitudinal thinning within the border tissue regions will precede the onset and progression of peripapillary microvascular drop out[11,21,22] and atrophy[11,23] in the aging, glaucomatous, and myopic eye. Our proposed method can enable longitudinal PCT measurements to be made in the internally and externally oblique border tissue regions of at-risk eyes, thereby allowing the clinical timing of longitudinal OCT PCT thinning and OCT angiographic[11,21,22] change to be assessed.

Methods

Conventions

A detailed description of our study participants and our methods of data acquisition has been previously published.[1] We use the term *ONH* to refer to the tissues that are contained within the scleral canal and those immediately adjacent to it (i.e., the peripapillary sclera, choroid, and retina as well as the retrolaminar optic nerve). PCT is the distance between the anterior scleral surface and Bruch's membrane and is always a positive number or zero. Factors that have positive and negative effects on PCT correlate to thicker and thinner PCT, respectively. Global PCT refers to PCT without regard to sector.

Participants

A total of 362 healthy individuals participated in this study[1]: 246 self-identified European descent,[24] 47 Hispanic ethnicity, 47 African descent, 19 Asian descent, and 3 Native American descent participants. The participants were recruited to represent the ethnic composition of the U.S. population[25] as mandated by the U.S. Food and Drug Administration. Consent documents approved by the institutional review board were signed by each participant. The study adhered to the Declaration of Helsinki for research involving human participants.

At the first visit, medical and ophthalmic histories were obtained, followed by anterior segment and external eye examinations, Van Herrick angle assessment, crystalline lens evaluation, standard Snellen or Early Treatment Diabetic Retinopathy Study visual acuity, refraction, central keratometry, and axial length assessments. Standard automated perimetry (Humphrey Field Analyzer [Carl Zeiss Meditec, Dublin, CA, USA], 24–2 Swedish Interactive Thresholding Algorithm), was repeated once if deemed unreliable or outside normal limits (see below). OCT examination, ophthalmoscopic examination of the posterior pole, and stereophotography were followed by Goldmann tonometry and pachymetry.

Inclusion criteria included age 18 to 90 years old; no history of glaucoma, IOP $\leq$ 21 mm Hg; best corrected visual acuity $\geq$ 20/40, refraction less than $\pm$6.00 diopter (D) sphere and $\pm$2.00 D cylinder; (4) Glaucoma Hemifield Test and mean deviation within normal limits. Exclusion criteria included unusable stereo photographs or insufficient OCT image quality (quality score $<$ 20); clinically abnormal optic disc appearance; any intraocular surgery (except uncomplicated cataract surgery) or vitreous, retinal, choroidal, or neurophthalmological disease; and ethnic group other than those listed. All test procedures were performed on both eyes of each participant, but only one eye was randomized for analysis.

OCT Image Acquisition and Segmentation

The ONH, peripapillary retinal nerve fiber layer (RNFL) and macula were imaged with spectral domain OCT (Spectralis, Heidelberg Engineering GmbH, Heidelberg, Germany; software version Heyex 1.9.10.0). For each eye, prior to image acquisition, refractive correction and keratometry values were entered into the instrument data base and the operator manually defined the fovea with a live B-scan, then centered the imaging field on the ONH, where the two BMO points in each of two perpendicular ONH radial B-scans were identified. These steps established the eye-specific, FoBMO axis that was used as the reference for the acquisition of all scans.[26] The complete ONH imaging pattern consisted of 24 radially equidistant, 15° B-scans (768 A-lines each) centered on the BMO and acquired in enhanced depth imaging[27] mode, with an average of 25 repetitions each.

Our strategy for OCT ONH image manual segmentation has been described previously (Fig. 1).[1] Raw OCT volumes along with automatic segmented BMO points were exported from the device and imported into our custom three-dimensional visualization and segmentation software (ATL 3D Suite).[28] ONH and peripapillary landmarks were manually segmented in each radial B-scan (24 total) of each OCT volume. Segmented landmarks included the internal limiting membrane, posterior surface of the RNFL, posterior surface of Bruch's membrane/

Investigative Ophthalmology & Visual Science

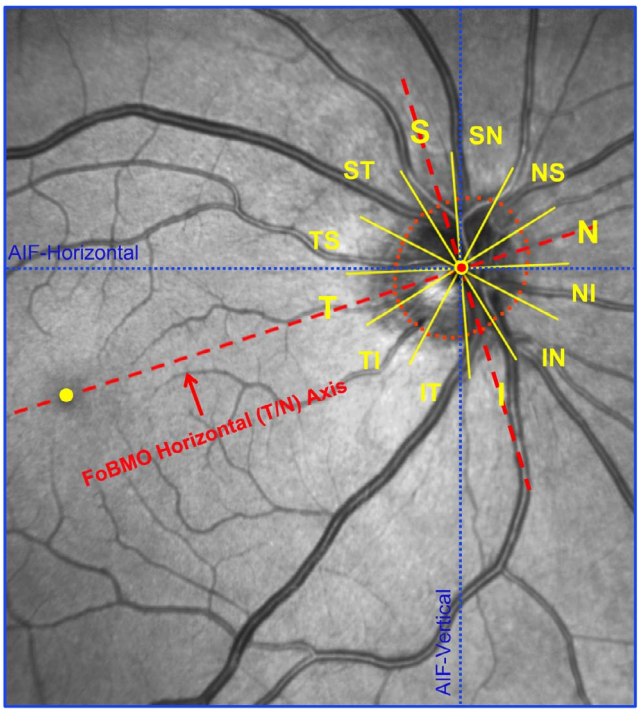

Figure 4. FoBMO 30° ONH sectors for a representative study eye (FDA056). The fovea (*yellow dot*) and four BMO points were anatomically identified using real-time OCT imaging at the time of image acquisition by the technician. The delineated BMO points from the 24 acquired OCT B-scans are projected onto the IR image along with the geometric center of BMO (BMO centroid - *red dot* with *yellow border*) so as to establish the foveal to BMO (FoBMO) axis. Twelve 30° (clock-hour) sectors were then established relative to the FoBMO axis. Note that the use of the FoBMO axis for orientation rather than the acquired image frame vertical and horizontal axes (*blue dotted lines*) means that the 12 FoBMO sectors were applied in an anatomically consistent fashion to each study eye.[24,26,58] S, superior; SN, superior nasal; NS, nasal superior; N, nasal; NI, nasal inferior; IN, inferior nasal; I, inferior; IT, inferior temporal; TI, temporal inferior; T, temporal; TS, temporal superior; ST, superior temporal.

retinal pigment epithelium complex, BMO, neural canal wall, anterior lamina cribrosa surface, anterior scleral surface, and the ASCO (segmented on each side of the canal by visually projecting the plane of the peripapillary anterior scleral surface through the neural canal wall and marking their intersection).[1] All manual segmentations were performed by observers at the Optic Nerve Head Research Laboratory, Devers Eye Institute (Portland, OR, USA).

PCT, Percent PCT (%PCT), and ASCO Area

Quantification of all parameters was performed within custom software (Matlab version 7.3.0.267; The MathWorks, Natick, MA, USA). All left eye data were converted to right eye configuration. For each OCT 24 radial B-scan data set, a plane was fit to the 48 segmented ASCO points (Fig. 1), satisfying a least mean square error restraint as previously described for both BMO and ASCO in a series of publications.[1,19] The Bruch's membrane, anterior scleral surface, and ASCO points were interpolated using B-splines. The interpolated Bruch's membrane points and anterior scleral surface points were then resampled at equal distances from BMO and the ASCO, respectively, allowing the consistent sampling of each surface between the original segmentation points.

PCT was measured at six distances from the ASCO (hereafter referred to as ASCO measurement distances: 100 μm [PCT-100], 300 μm [PCT-300], 500 μm [PCT-500], 700 μm [PCT-700], 900 μm [PCT-900], and 1100 μm [PCT-1100]) measured within the ASCO reference plane and projected to the anterior scleral surface (Fig. 2). At each anterior scleral measurement point, PCT was defined by the minimum distance to the posterior surface of Bruch's membrane. However, when internally or externally oblique border tissues were present in a given study eye (Fig. 3), PCT measurements within the regions of internally and externally oblique border tissues (most often at the 100 μm and 300 μm measurement points) were not included in the normative values because the density of the border tissues themselves and the adjacent choroidal septa made the presence of active choroidal vasculature difficult to determine. Global and sectoral %PCT were calculated for each study eye, at each ASCO distance, as the PCT divided by the mean PCT of the study population at that location. ASCO area was calculated after projection of the ASCO points onto the ASCO reference plane, as previously reported.[1]

Regionalization

Twelve 30° sectors (centered on each clock hour) were established relative to the FoBMO axis as previously described (Fig. 4).[1,26]

Interobserver Reproducibility

Interobserver segmentation reproducibility was assessed at each PCT measurement distance by having four observers each segment the same eight OCT data sets. For each OCT data set, global and sectoral values for PCT at all six ASCO measurement distances were computed for each observer. Interobserver reproducibility for ASCO area has been previously reported.[1]

Statistical Analysis

All statistical analyses were performed in R version 3.1.3 (The R Foundation for Statistical Computing, Vienna, Austria). Intraclass correlation coefficients (ICC) between observers for each global and sectoral parameter (i.e., one global value and 12 sectoral value per distance per participant per observer) were calculated using a 2-way analysis of variance (ANOVA).[29,30]

The effects of measurement distance from the ASCO, age, axial length, sex, ethnicity, and IOP on overall global PCT were assessed within an ANOVA by general linear model using generalized estimation equation (GEEGLM). Univariate regression models were formed to relate global PCT at each measurement location with age, ASCO area, axial length, and IOP. The significance and magnitude of the effects of age, axial length, ASCO area, IOP, sex, and ethnicity on global PCT at each measurement location were assessed by calculating the proportion of the total variance (R^2) within an ANOVA with a linear regression model. Coefficients for each of these effects on global choroidal thickness at each measurement location were also assessed within a multivariate linear regression model.

For sectoral PCT, an initial overall ANOVA was performed with a generalized estimation equation model to assess the significance of age, ASCO area, axial length, sex, ethnicity, sector, ASCO distance, sector versus age, measurement distance versus age, measurement distance versus sector, and distance versus sector versus age. A follow-up ANOVA was then performed to assess the significance of age, ASCO area, axial length, sex, ethnicity, sector, and sector-versus-age effects on sectoral choroidal thickness at each measurement location.

Investigative Ophthalmology & Visual Science

Table 1. Demographic and Ocular Characteristics of the Study Participants

Characteristics	All Subjects, $n = 362$	European Hispanic Descent, $n = 246$	Hispanic Ethnicity, $n = 47$	African Descent, $n = 47$	Asian and Native American Descent, $n = 22$*	ANOVA or Chi-Square Test, P Value†
Female, n (%)	202 (56)	137 (56)	30 (64)	22 (47)	13 (59)	0.41‡
Left eye, n (%)	181 (50)	123 (50)	24 (51)	25 (53)	9 (41)	0.83‡
Age, y (SD)	50.62 (17.53)	52.17 (18.27)	45.28 (14.07)	49.40 (14.76)	47.27 (19.25)	0.06
Axial length, mm (SD)	23.74 (0.95)	23.67 (0.91)	23.87 (1.02)	23.80 (1.03)	24.07 (1.11)	0.18
ASCO area, mm^2 (SD)	2.23 (0.43)	2.21 (0.44)	2.31 (0.45)	2.21 (0.41)	2.30 (0.38)	0.40
IOP, mm Hg (SD)	14.53 (2.70)	14.56 (2.71)	14.27 (2.67)	14.91 (2.73)	13.95 (2.54)	0.49
CCT, μm (SD)	555.31 (32.60)	555.49 (34.52)	555.71 (25.99)	545.60 (29.09)	573.21 (22.01)	0.01
Spherical equivalent, D (SD)	−0.47 (1.82)	−0.29 (1.72)	−0.43 (1.90)	−0.78 (1.77)	−1.93 (2.14)	<0.0001

CCT, central corneal thickness; D, diopters.
* A total of 19 (5.2%) Asians and 3 (0.8%) Native Americans.
† ANOVA or chi-square test to check if ethnicity is significant different for a demographic parameter.
‡ Chi-square test.

These two ANOVA analyses were also performed on sectoral %PCT data. Finally, within sectoral PCT and sectoral %PCT data, comparisons between the sectors with the three largest thickness values and the sectors with the three smallest thickness values or between the sectors with the three fastest and three slowest age-related change rates were performed with a generalized estimation equation model. Statistical significance was assumed when $P \leq 0.05$.

Results

Demographic and ocular data for all 362 participants are summarized in Table 1. Because there were very few Asian and Native American descent participants, ethnicity was reduced to four groups (European descent, Hispanic ethnicity, African descent, and combined Asian and Native American descent) for subsequent analyses. Five participants (1.4%) were excluded from the analysis of PCT because of poor visualization of the anterior scleral surface at all measurement distances. A total of 48 participants (13.3%) and 5 participants (1.4%) were excluded from the analysis at the 100 and 300 μm measurement distances, respectively, as a result of externally oblique border tissues that extended beyond these measurement points (Fig. 3). A total of 12 participants (3.3%) were excluded from the analysis at the 1100 μm measurement distance as a result of the B-scans not extending to this distance. Age, axial length, ASCO area, and IOP were not significantly different by ethnicity (ANOVA, P values ≥ 0.05). The proportion of females and left eyes were not significantly different (χ^2 test, $P = 0.41$). Central cornea thickness and spherical equivalent were statistically different among the ethnic groups (ANOVA, $P \leq 0.05$; Table 1).

Interobserver Reproducibility

Between-observer ICC values for all parameters assessed globally ranged from 0.83 to 0.96 and sectorally were ≥ 0.8 for all sectors at measurement distances ≥ 300 μm, except for the nasal–superior sector at the 300 μm measurement point, where the ICC was 0.78. Sectoral ICCs at the 100 μm measurement point were lower, ranging from 0.62 to 0.86, except for the temporal sector (ICC 0.57).

Global PCT

Global PCT was significantly influenced by age, ASCO area, axial length, ethnicity, measurement distance from the ASCO, sex, and the interactions between measurement distance versus age by ANOVA ($P \leq 0.05$, GEEGLM).

Global PCT by Distance From ASCO

Population means, medians, confidence intervals, and ranges for global PCT at each measurement distance are reported in Table 2. Mean PCT was 108.81 μm at the PCT-100 measurement point and increased to 172.47 μm at the PCT-1100 measurement point. In the univariate regression models, age was negatively associated with PCT at all distances ($P < 0.0001$; R^2 values for each model ranging from 0.13–0.16; Fig. 5). The effect of age on PCT became more pronounced with increasing distance (–0.59 μm/year at PCT-100, progressively increasing to –1.43 μm/y at PCT-1100; Fig. 5). Axial length was weakly negatively associated with PCT at all distances ($P < 0.01$; R^2 values for each model ranging from 0.02–0.06; Supplementary Fig. S1).

Table 2. Global Mean PCT at Each Measurement Distance From the ASCO

Measurement Location*	Number of Eyes†	Mean	SD	Minimum	5% Percentile	Median	95% Percentile	Maximum
PCT-100	309	108.81	26.25	44.41	65.38	107.4	150.72	193.11
PCT-300	352	129.30	37.46	37.6	66.27	128.75	192.05	242.60
PCT-500	357	144.12	46.71	34.86	68.18	143.2	225.1	267.29
PCT-700	357	156.45	53.88	36.41	71.22	154.4	252.64	295.84
PCT-900	357	166.08	58.97	38.81	75.86	164.3	270.06	322.81
PCT-1100	345	172.47	62.41	40.32	75.31	169.6	281.98	340.71

* Measured relative to the ASCO.
† Number of eyes with data at each measurement point (see the Results and Discussion).

Investigative Ophthalmology & Visual Science

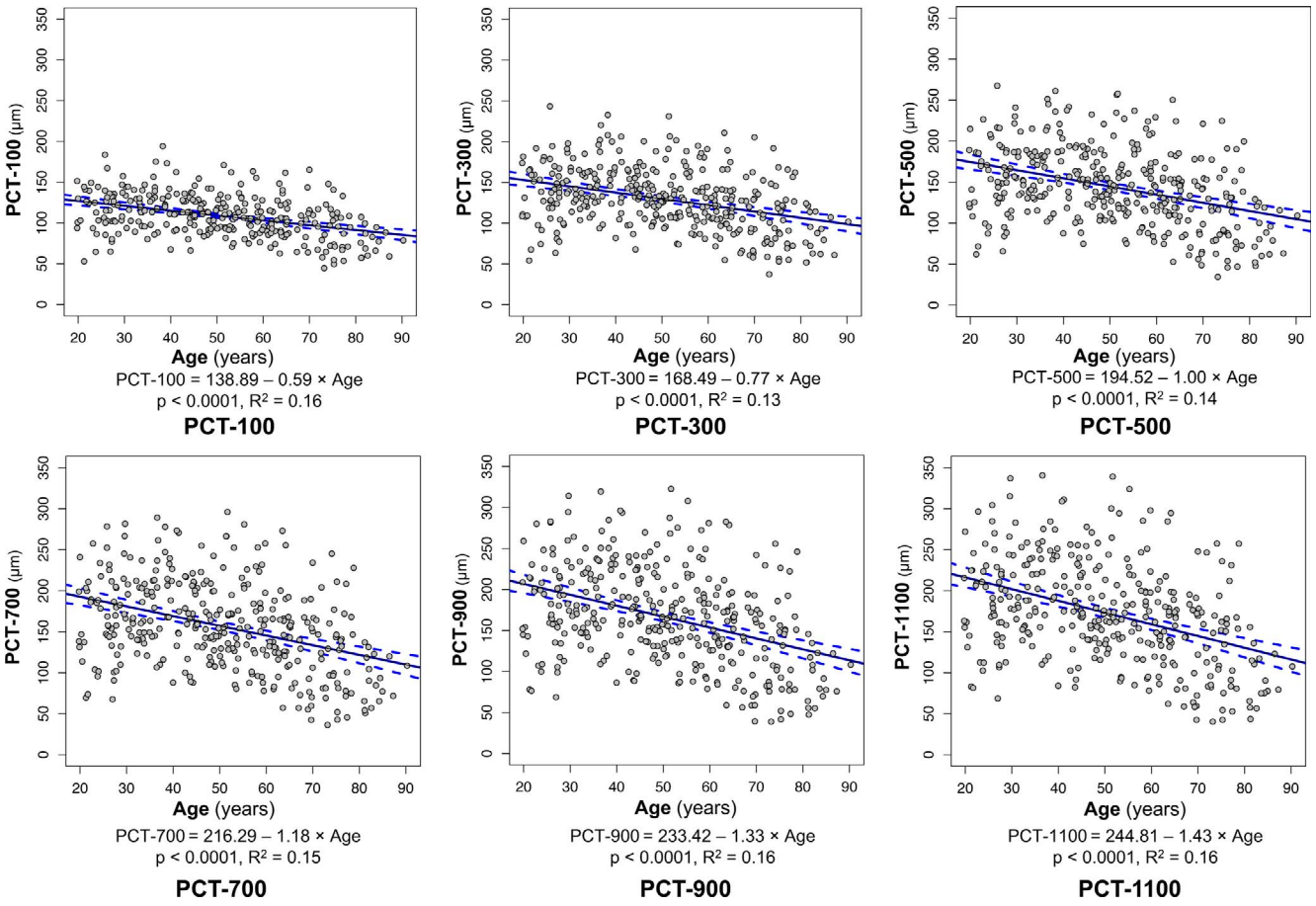

Figure 5. Scatterplot and univariate linear regression of PCT and age at each measurement point. Panels depict data at the 100, 300, and 500 μm measurement distances above and the 700, 900, and 1100 μm distances below. The slope of the regression line achieved significance at the $P < 0.0001$ level at all distances from the ASCO. *Solid blue lines* indicate fitted linear regression lines; *dotted blue curves* indicate the 95% CI of the regression lines; *gray circles* with *black border* indicate individual eye values.

Table 3. Multivariable Regression Coefficients for Demographic, Ocular, Sex, and Ethnicity Effects on PCT at Each Measurement Distance From the ASCO

	PCT-100		PCT-300		PCT-500		PCT-700		PCT-900		PCT-1100	
Parameter	**Coefficient**	**SE**	**Coefficient**	**SE**	**Coefficient**	**SE**	**Coefficient**	**SE**	**Coefficient**	**SE**	**Coefficient**	**SE**
Intercept	**295.14**	36.69	**472.55**	45.98	**612.77**	55.21	**711.54**	62.91	**783.92**	68.52	**818.43**	72.91
Age	**−0.62**	0.08	**−0.87**	0.10	**−1.14**	0.12	**−1.35**	0.14	**−1.51**	0.15	**−1.63**	0.16
Axial length	**−6.02**	1.50	**−11.7**	1.83	**−15.93**	2.19	**−18.93**	2.49	**−21.13**	2.71	**−21.64**	2.90
ASCO area	−6.10	3.19	**−11.4**	3.96	**−15.27**	4.80	**−16.95**	5.47	**−17.6**	5.96	**−22.43**	6.83
IOP	−0.21	0.48	−0.33	0.62	−0.73	0.75	−0.92	0.85	−1.04	0.93	−1.04	1.00
Sex (male vs. female)*	4.83	2.72	6.16	3.45	**8.86**	4.15	**11.07**	4.73	**12.4**	5.15	**12.54**	5.53
Ethnicity and race												
Hispanic ethnicity‡ vs. European descent†	**10.65**	4.06	**19.35**	5.19	**25.30**	6.22	**30.04**	7.09	**32.67**	7.72	**34.75**	8.42
African descent‡ vs. European descent†	**9.90**	4.02	**27.64**	5.13	**36.33**	6.22	**41.57**	7.09	**43.15**	7.72	**43.79**	8.17
Asian and Native American descent vs. European descent†	−4.56	6.21	−3.59	7.22	−4.42	8.57	−6.81	9.77	−9.27	10.64	−9.95	11.25

Bold indicates $P \leq 0.05$.

* Parameter in the male participants was compared to the same parameter in the reference female participants.

† Parameters in African descent, Hispanic ethnicity, and Asian and Native American descent participants were compared with the same parameters in reference European descent participants separately.

‡ African descent and Hispanic ethnicity participants were not significantly different overall or at any measurement distance.

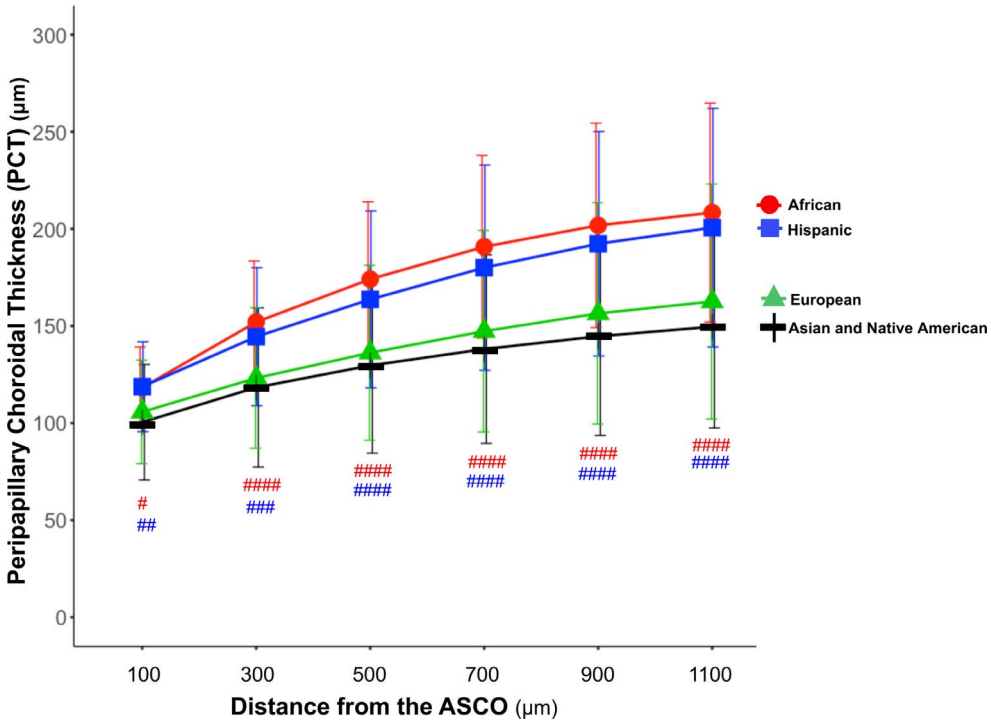

Figure 6. PCT by ethnicity and distance from the ASCO. The mean (± standard deviation) PCT for the four ethnicity groups are plotted for the six measurement distances from the ASCO. PCT was compared between European, Hispanic, and African descent ethnicities. PCT was thicker in the African descent and Hispanic ethnicity groups when compared with the European descent group, respectively, at all six distances from the ASCO (Table 3). *P* values by general linear regression by general estimation equation model are depicted for each comparison in *red* or *blue* as follows: ####$P < 0.0001$; ###$P < 0.001$; ##$P < 0.01$; #$P < 0.05$). The differences between the African descent and Hispanic ethnicity groups did not achieve significance.

In multivariable analysis, increased age and axial length were negatively associated with PCT at all measurement distances (Table 3, model $R^2 = 0.23$–0.34). Increased ASCO area was also negatively associated with PCT for all distances ≥300 µm from the ASCO. PCT was thicker in eyes of African descent and Hispanic ethnicity at all measurement distances than European descent eyes (PCT-100: African 118.27 ± 20.91 µm, Hispanic 118.74 ± 23.13 µm, European 105.76 ± 26.65 µm; PCT-1100: African 208.39 ± 56.35 µm, Hispanic 200.62 ± 61.45 µm, European 162.58 ± 60.53 µm; $P \leq 0.01$; Fig. 6). Differences between the African descent and Hispanic ethnicity groups did not achieve statistical significance at any distances ($P = 0.173$ to 0.887). The effectors that contributed most to explaining the variability of global PCT at each measurement distance were age (ranging from 13%–16%), axial length (ranging from 4%–10%), ethnicity (ranging from 2%–6%), ASCO area (ranging from 1%–2%), and sex (1%), respectively.

Sectoral PCT

PCT was thinnest within the inferior–nasal, inferior, inferior–temporal, and temporal sectors at all measurement distances (Fig. 7, upper row). The sectors with the thinnest PCT were significantly different from the sectors with the thickest PCT at all measurement distances (Fig. 7, upper row; $P \leq 0.05$, general linear regression by GEEGLM).

The effect of sector on PCT remained significant after adjusting for all other effectors at each measurement distance (ANOVA; Supplementary Table S1). Sectoral PCT was significantly influenced by age, ASCO area, axial length, ethnicity, sex, sector, measurement distance from the ASCO, and the interactions between sector versus age, measurement distance versus age, measurement distance versus sector, and measurement distance versus sector versus age, by ANOVA (by GEEGLM, $P \leq 0.05$). In a separate ANOVA (Supplementary Table S2), the effect of age and the effect of the sector-versus-age interaction on the %PCT were also significant at all measurement distances.

The thinnest sectors (upper row of Fig. 7) also demonstrated the most rapid thinning with age (middle and lower panels, Fig. 7). At all six measurement distances, the effects of age on PCT and %PCT in the sectors with the fastest rate of age-related thinning were significantly greater ($P \leq 0.05$, general linear regression by GEEGLM model) than the effects of age in the sectors with the slowest rates of age-related thinning (Fig. 7, middle and lower rows). Age-related PCT reduction was from 15.6% to 20.7% greater in the faster sectors when compared with the slower sectors at six measurement distances.

Although the sectoral distribution of PCT was similar at all measurement distances (thinnest inferiorly and inferior temporally; Fig. 7, upper row), sectoral thickness variation increased substantially as the measurement distance from the ASCO increased. Sectoral PCT ranged from 101 to 115 µm at the PCT-100 µm measurement location and ranged from 143 to 189 µm at the PCT-1100 µm measurement location. Age-affected sectoral PCT (Fig. 7, middle row) and %PCT (Fig. 7, lower row) also increased in magnitude and variation as the distance from ASCO increased. Sectoral age effects on %PCT ranged from –0.52 to –0.69 %/y at the PCT-100 µm measurement location and from –0.86 to –1.18 %/y at the PCT-1100 µm measurement location.

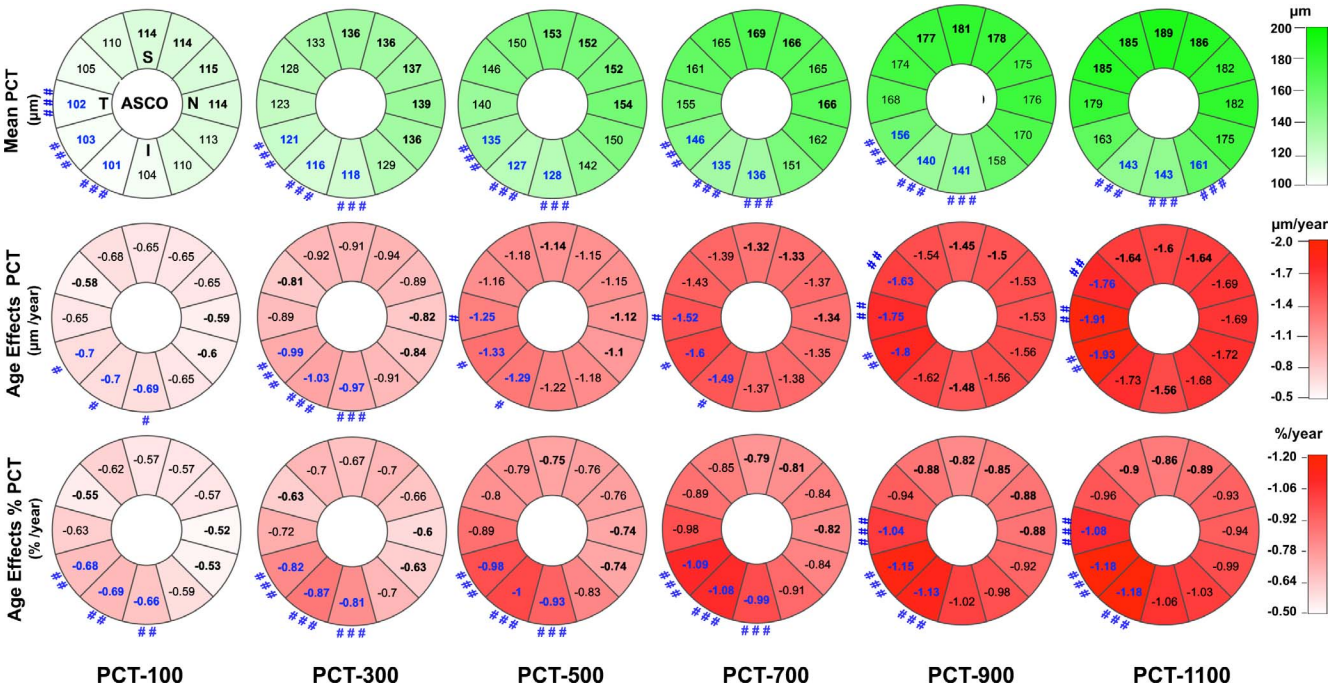

Figure 7. FoBMO sectoral mean PCT (*upper row*), age-related PCT change (*middle row*), and age-related percent PCT change (%PCT, *lower row*) at six proximal (PCT-100 μm) to distal (PCT-1100 μm) locations from the ASCO. Data are presented in right eye orientation (*upper left*) by 30° (clock-hour) sectors that are oriented relative to the FoBMO axis. The mean PCT within each sector at six measurement locations (extending from 100 μm from the ASCO (*left most column*) to 1100 μm from the ASCO (*right most column*) are shown (*upper row*). The mean PCT of the top three thickest sectors at each measurement distance are *bold black*. The mean PCT of the top three thinnest sectors are *bold blue*. The thinnest sectors are significantly thinner than the thickest sectors when they are accompanied by a *number sign* symbol (see below). The rate of PCT change with age in each sector (μm/y), after adjusting for axial length, ASCO area, IOP, ethnicity, and sex (*middle row*). The sectors with the top three slowest rates of change are *bold black*. The sectors with the top three fastest rates of change are *bold blue*. The rates of change of the fastest sectors are significantly faster than the slowest sectors when they are accompanied by a *number sign* symbol (legend below). The rate of %PCT change with age in each sector after adjusting for the same covariates (*lower row*). The sectors with the three lowest rates of %PCT change are *bold black*. The sectors with the three fastest rates of %PCT change are shown in *bold blue*. The fastest sectors are significantly faster than the slowest sectors when accompanied by a *number sign* symbol. Significant differences, by a general estimation equation model are depicted by ###$P < 0.001$; ##$P < 0.01$; and #$P < 0.05$, respectively.

Discussion

This study characterizes PCT in a large healthy population and introduces both the use of the ASCO as the neural canal reference opening for its measurement and the use of the FoBMO axis as the common horizontal axis for its regionalization. Our findings suggest that OCT PCT is thinnest in the inferior temporal sectors and thinnest closest to the ASCO. Thinner PCT was associated with age, axial length, European descent, and weakly associated with larger ASCO area and female sex, respectively. Among these effects, age had the strongest influence, and its effect was greatest within the inferior temporal sectors. Although the clinical significance of the effects we describe remains to be determined, our approach to quantifying PCT as well as the findings we report provide a foundation for incorporating PCT into existing OCT strategies to diagnose and follow optic neuropathies. Our approach has also yielded sectoral data that gives an indication of the changes in PCT to be expected with normal aging against which disease-related changes can be gauged.[1,24,31]

In general, the PCT values we report are similar to the existing literature, although among all previous studies there are differences in scan pattern and location, imaging device, age distribution, ethnicity, and reference point (most being relative to BMO or derived from standard RNFL circle scans). Rhodes et al.[32] reported an average PCT ranging from 63.9 μm (0–250 μm from BMO) to 164.8 μm (1000–1500 μm from BMO) in 166 normal eyes of European and African descent participants using a Spectralis OCT 24 radial B-scan pattern. Lee et al.[17] reported an average PCT to be 135.6 μm in 48 normal Korean eyes 500 μm from the border tissues of Elschnig using a Topcon swept source OCT and a 12 B-scan pattern. However, Park et al.[15] reported an average PCT to be 226.35 μm in 48 healthy Korean participants within the region of the choroid 300 to 1800 μm from BMO using a Spectralis OCT and a 6 B-scan ONH radial pattern.

The thickness in the Park et al.[15] study was larger than our data obtained 1100 μm from the ASCO, larger than the average thicknesses of most other studies and may be a reflection of the longer sampling distance from BMO in that study (because choroidal thickness increases progressively as the distance from BMO or ASCO increases). Although it may also be the case that the choroid is thicker in Korean eyes, Chung et al.[33] measured PCT using Spectralis circle scans in 87 healthy Korean eyes and reported an average thickness of 157.3 μm, which is within the confidence intervals of our measurements at 900 and 1000 μm (roughly the position of a standard circle scan within our data). Several other studies have reported global PCT within standard 12° (or 3.4 mm diameter) circle scans in a wide variety of healthy participants that varies from 130 μm to 167 μm,[34–42] which are again within the confidence intervals of our measurements at the PCT-900 μm and PCT-1000 μm measurement points.

The peripapillary choroid was thinnest within the inferior sectors of our study eyes, which agrees with a series of previous reports.[15,17,32,34,41,43,44] However, our finding that

age-related peripapillary choroidal thinning was greatest within the inferior temporal sectors has not previously been reported. This finding complements a growing literature that suggests that age-related changes in the neuroretinal rim[24,45] and RNFL[24] are greatest within the inferior temporal region of the ONH, where glaucomatous damage is thought to be most frequent.[46] In contrast, a recent study in a healthy Japanese population found age effects on the rim and RNFL tissues to be greatest in the superior nasal rather than the inferior temporal sectors.[31] Because our approach also quantifies ONH rim tissue and RNFL measurements, this will afford longitudinal studies to determine the relative timing and sectoral correlation of choroidal ONH rim tissue and RNFL thinning in aging and glaucoma to be performed.

Many previous studies have reported that increasing age is associated with a thinner peripapillary choroid.[16,17,32,34,41] In our study, age played the largest role in explaining the variance in PCT (from 13%–16% depending on the distance from the ASCO). After adjusting for other significant effectors, age-related decline in global peripapillary choroid thickness ranged from −0.62 μm per year 100 μm from the ASCO to −1.63 μm per year 1100 μm from the ASCO, which is similar to the rates reported in other studies.[16,17,32,34,41]

Axial length demonstrated the second most important influence on PCT in our study. Several studies have reported that longer axial length is associated with thinner peripapillary choroid in normal eyes.[32,38,40] However, given our inclusion criteria for refractive error and axial length, we excluded highly myopic eyes. The relationship between PCT and axial length may have been stronger with the inclusion of highly myopic eyes. Other significant influences in our study included ethnicity, ASCO area, and sex, although male eyes demonstrated only slightly thicker PCT, which achieved significance at the most distal measurement locations. We found PCT to be thicker in African descent and Hispanic ethnicity participants at all distances from the ASCO. Rhodes et al.[32] previously reported thicker choroidal thickness in African descent eyes when compared with European descent eyes at all distances from the BMO.

The limitations of this study include the relatively small number of non-European descent participants, which will be addressed by completion of PCT measurements in 258 healthy Japanese participants,[31] completion of ongoing African descent and Hispanic ethnicity group expansions to 250 participants each, and the eventual completion of a planned study of 250 healthy participants from mainland China. Because of the heterogeneous nature of Hispanic ethnicity, the fact that PCT differences between the African descent and Hispanic ethnicity groups did not achieve significance may have been the result of the presence of a substantial amount of African heritage in the participants who self-identified as Hispanic in this study. Additional studies in a variety of African descent and Hispanic ethnicity participants are required.

In this article (and the article that precedes it[1]), we identified the ASCO by projecting the immediate peripapillary scleral surface through the border tissues of Elschnig to the neural canal wall boundary (Fig. 2). Unlike BMO, which is an anatomically identifiable structure in most nonmyopic[18] eyes by histology and by OCT,[19,47,48] the ASCO is not an anatomically identifiable structure in either modality. Instead the ASCO must be estimated, rather than anatomically identified, as outlined previously. However, interoperator reproducibility of global ASCO area and PCT relative to ASCO was excellent in this study. Altough the reproducibility of choroidal thickness was generally good sectorally, it was diminished for the 100 μm measurement point in those sectors where the peripapillary choroid was thinnest. The importance of including the ASCO in human ONH phenotyping has been previously discussed.[1] Studies that seek predictive relationships between cross-sectional PCT, longitudinal PCT change, peripapillary atrophy, and glaucomatous or myopic rim and RNFL loss are indicated. In these studies, the effect of using ASCO versus BMO as the reference opening for the measurement should also be assessed.

Finally, to ensure that our most important findings were preserved, we recalculated PCT measurements at the same measurement distances from BMO (Supplementary Fig. S2) instead of from the ASCO. Comparing the BMO-based PCT values in Supplementary Table S3 to the ASCO-based PCT values in Table 2, the progressive increase in PCT from the scleral canal to the macula is still present. However, there are less BMO PCT-100 measurement values when compared with the number of ASCO PCT-100 values, and the BMO PCT values are modestly smaller than the ASCO PCT values at all measurement points. Comparing sectoral age effects using ASCO as the reference (Fig. 7) to sectoral age effects using BMO (Supplementary Fig. S3) reveals identical trends in both analyses, although the higher inferior temporal sectoral age effects achieve significance at the ASCO PCT-100 measurement point but do not achieve statistical significance at the BMO PCT-100 measurement point. We believe that these differences are a direct result of internally oblique border tissues being more common and extensive than externally oblique border tissues in human eyes.[20] In the setting of internally oblique border tissues, the BMO PCT measurement points, at every measurement distance, fall closer to the scleral canal than the ASCO PCT measurement points of equal distance. As a consequence, more BMO PCT 100 measurement points fall within internally oblique border tissues (and as a result are excluded), and the BMO PCT measurements at all distances from the BMO are closer to the ONH, and thus smaller than the ASCO PCT measurements of equal distance.

In summary, the OCT PCT was thinnest within the inferior temporal sectors, and thinner PCT was most strongly associated with older age, axial length, and European descent and weakly associated with larger ASCO area and female sex. Among these effects, age had the strongest influence, and its effect was greatest within the inferior temporal sectors. Although the clinical significance of our findings remain to be determined, our techniques provide a foundation for incorporating PCT into strategies for detecting and staging the optic neuropathies of human aging,[1,10,24,31,45,49] pathologic myopia,[4–8] and glaucoma.[50–54]

Acknowledgments

Partial material was previously presented at the Association for Research in Vision and Ophthalmology (ARVO) Annual Meeting, Baltimore, Maryland, United States, May 2017.

The authors thank Juan Reynaud for his OCT technical assistance, Lirong Qin and Luke Ryes for their help with reproducibility delineations, and Julia Monaghan at the Devers Eye Institute for assistance with manuscript preparation and submission.

Supported by National Eye Institute Grants NIH/NEI R01-EY021281 (CFB) and NIH/NEI R01-EY-019674 (SD), with supplemental support from Legacy Good Samaritan Foundation and Heidelberg Engineering, GmbH, Heidelberg, Germany.

Disclosure: **H. Yang**, None; **H. Luo**, None; **S.K. Gardiner**, None; **C. Hardin**, None; **G.P. Sharpe**, None; **J. Caprioli**, None; **S. Demirel**, Legacy Good Samaritan Foundation (F), Carl Zeiss Meditec (F), Heidelberg Engineering (F); **C.A. Girkin**, Heidelberg Engineering (F); **J.M. Liebmann**, Carl Zeiss Meditec (F), Topcon, Inc. (F) Alcon Laboratories (F), Allergan, Inc. (F), Diopsys Corporation (F), Glaukos Corporation (F), Heidelberg Engineering (F), Merz Pharmaceutical, Inc. (F), Optovue, Inc. (F), Quark Pharmaceuticals, Inc. (F), SOLX, Inc. (F); **C.Y. Mardin**, Heidelberg

Engineering (F); **H.A. Quigley**, Heidelberg Engineering (F); **Alexander F. Scheuerle**, Heidelberg Engineering (F); **B. Fortune**, Legacy Good Samaritan Foundation (F), Inotek Pharmaceuticals (F); **B.C. Chauhan**, Heidelberg Engineering (F, C, R); **C.F. Burgoyne**, Legacy Good Samaritan Foundation (F), Heidelberg Engineering (F, C, R)

References

1. Luo H, Yang H, Gardiner SK, et al. Factors influencing central lamina cribrosa depth: a multicenter study. *Invest Ophthalmol Vis Sci*. 2018;59:2357–2370.
2. Hayreh SS, Jonas JB, Zimmerman MB. Parapapillary chorioretinal atrophy in chronic high-pressure experimental glaucoma in rhesus monkeys. *Invest Ophthalmol Vis Sci*. 1998;39:2296–2303.
3. Hayreh SS, Pe'er J, Zimmerman MB. Morphologic changes in chronic high-pressure experimental glaucoma in rhesus monkeys. *J Glaucoma*. 1999;8:56–71.
4. Vianna JR, Malik R, Danthurebandara VM, et al. Beta and gamma peripapillary atrophy in myopic eyes with and without glaucoma. *Invest Ophthalmol Vis Sci*. 2016;57:3103–3111.
5. Hayashi K, Tomidokoro A, Lee KY, et al. Spectral-domain optical coherence tomography of beta-zone peripapillary atrophy: influence of myopia and glaucoma. *Invest Ophthalmol Vis Sci*. 2012;53:1499–1505.
6. Park HY, Shin HY, Park CK. Imaging the posterior segment of the eye using swept-source optical coherence tomography in myopic glaucoma eyes: comparison with enhanced-depth imaging. *Am J Ophthalmol*. 2014;157:550–557.
7. Ohno-Matsui K, Akiba M, Ishibashi T, Moriyama M. Observations of vascular structures within and posterior to sclera in eyes with pathologic myopia by swept-source optical coherence tomography. *Invest Ophthalmol Vis Sci*. 2012;53:7290–7298.
8. Ng DS, Cheung CY, Luk FO, et al. Advances of optical coherence tomography in myopia and pathologic myopia. *Eye (Lond)*. 2016;30:901–916.
9. Hayreh SS, Revie IH, Edwards J. Vasogenic origin of visual field defects and optic nerve changes in glaucoma. *Br J Ophthalmol*. 1970;54:461–472.
10. Burgoyne CF. A biomechanical paradigm for axonal insult within the optic nerve head in aging and glaucoma. *Exp Eye Res*. 2011;93:120–132.
11. Lee EJ, Lee KM, Lee SH, Kim TW. Parapapillary choroidal microvasculature dropout in glaucoma: a comparison between optical coherence tomography angiography and indocyanine green angiography. *Ophthalmology*. 2017;124:1209–1217.
12. Hayreh SS. Blood supply of the optic nerve head and its role in optic atrophy, glaucoma, and oedema of the optic disc. *Br J Ophthalmol*. 1969;53:721–748.
13. Cioffi GA, Van Buskirk EM. Vasculature of the anterior optic nerve and peripapillary choroid. In: Ritch R, Shields MB, Krupin T, eds. *The Glaucomas*. St. Louis: Mosby; 1996:177–197.
14. Sugiyama K, Cioffi GA, Bacon DR, Van Buskirk EM. Optic nerve and peripapillary choroidal microvasculature in the primate. *J Glaucoma*. 1994;3Suppl 1:S45–S54.
15. Park HY, Lee NY, Shin HY, Park CK. Analysis of macular and peripapillary choroidal thickness in glaucoma patients by enhanced depth imaging optical coherence tomography. *J Glaucoma*. 2014;23:225–231.
16. Johnstone J, Fazio M, Rojananuangnit K, et al. Variation of the axial location of Bruch's membrane opening with age, choroidal thickness, and race. *Invest Ophthalmol Vis Sci*. 2014;55:2004–2009.
17. Lee KM, Lee EJ, Kim T-W. Juxtapapillary choroid is thinner in normal-tension glaucoma than in healthy eyes. *Acta Ophthalmologica*. 2016;94:e697–e708.
18. Zheng F, Wu Z, Leung CKS. Detection of Bruch's membrane opening in healthy individuals and glaucoma patients with and without high myopia. *Ophthalmology*. 2018;125:1537–1547.
19. Strouthidis NG, Yang H, Fortune B, Downs JC, Burgoyne CF. Detection of optic nerve head neural canal opening within histomorphometric and spectral domain optical coherence tomography data sets. *Invest Ophthalmol Vis Sci*. 2009;50:214–223.
20. Reis AS, Sharpe GP, Yang H, Nicolela MT, Burgoyne CF, Chauhan BC. Optic disc margin anatomy in patients with glaucoma and normal controls with spectral domain optical coherence tomography. *Ophthalmology*. 2012;119:738–747.
21. Shin JW, Kwon J, Lee J, Kook MS. Choroidal microvasculature dropout is not associated with myopia, but is associated with glaucoma. *J Glaucoma*. 2018;27:189–196.
22. Suh MH, Zangwill LM, Manalastas PI, et al. Deep retinal layer microvasculature dropout detected by the optical coherence tomography angiography in glaucoma. *Ophthalmology*. 2016;123:2509–2518.
23. Hamasaki DI, Fujino T. Effect of intraocular pressure on ocular vessels. Filling with India ink. *Arch Ophthalmol*. 1967;78:369–379.
24. Chauhan BC, Danthurebandara VM, Sharpe GP, et al. Bruch's membrane opening minimum rim width and retinal nerve fiber layer thickness in a normal white population: a multicenter study. *Ophthalmology*. 2015;122:1786–1794.
25. Bureau USC. *Statistical Abstract of the United States: 2012*. U.S. Census Bureau. Available at www.census.gov. Accessed February 14, 2019.
26. He L, Ren R, Yang H, et al. Anatomic vs. acquired image frame discordance in spectral domain optical coherence tomography minimum rim measurements. *PLoS One*. 2014;9:e92225.
27. Spaide RF, Koizumi H, Pozzoni MC. Enhanced depth imaging spectral-domain optical coherence tomography. *Am J Ophthalmol*. 2008;146:496–500.
28. Fortune B, Reynaud J, Hardin C, Wang L, Sigal IA, Burgoyne CF. Experimental glaucoma causes optic nerve head neural rim tissue compression: a potentially important mechanism of axon injury. *Invest Ophthalmol Vis Sci*. 2016;57:4403–4411.
29. Shrout PE, Fleiss JL. Intraclass correlations: uses in assessing rater reliability. *Psychol Bull*. 1979;86:420–428.
30. McGraw KO, Wong SP. Forming inferences about some intraclass correlation coefficients. *Psychol Method*. 1996;1:30–46.
31. Araie M, Iwase A, Sugiyama K, et al. Determinants and characteristics of Bruch's membrane opening and Bruch's membrane opening-minimum rim width in a normal Japanese population. *Invest Ophthalmol Vis Sci*. 2017;58:4106–4113.
32. Rhodes LA, Huisingh C, Johnstone J, et al. Peripapillary choroidal thickness variation with age and race in normal eyes. *Invest Ophthalmol Vis Sci*. 2015;56:1872–1879.
33. Chung HS, Sung KR, Lee KS, Lee JR, Kim S. Relationship between the lamina cribrosa, outer retina, and choroidal thickness as assessed using spectral domain optical coherence tomography. *Korean J Ophthalmol*. 2014;28:234–240.
34. Huang W, Wang W, Zhou M, et al. Peripapillary choroidal thickness in healthy Chinese subjects. *BMC Ophthalmol*. 2013;13:23.
35. Tornow RP, Schrems WA, Bendschneider D, et al. Atypical retardation patterns in scanning laser polarimetry are associated with low peripapillary choroidal thickness. *Invest Ophthalmol Vis Sci*. 2011;52:7523–7528.

Investigative Ophthalmology & Visual Science

36. Lin Z, Huang S, Xie B, Zhong Y. Peripapillary choroidal thickness and open-angle glaucoma: a meta-analysis. *J Ophthalmol*. 2016;2016:5484568.
37. Ersoz MG, Mart DK, Ayintap E, et al. The factors influencing peripapillary choroidal thickness in primary open-angle glaucoma. *Int Ophthalmol*. 2016;37:827–833.
38. Jiang R, Wang YX, Wei WB, Xu L, Jonas JB. Peripapillary choroidal thickness in adult Chinese: The Beijing Eye Study. *Invest Ophthalmol Vis Sci*. 2015;56:4045–4052.
39. Li L, Bian A, Zhou Q, Mao J. Peripapillary choroidal thickness in both eyes of glaucoma patients with unilateral visual field loss. *Am J Ophthalmol*. 2013;156:1277–1284.e1.
40. Hirooka K, Tenkumo K, Fujiwara A, Baba T, Sato S, Shiraga F. Evaluation of peripapillary choroidal thickness in patients with normal-tension glaucoma. *BMC Ophthalmol*. 2012;12:29.
41. Roberts KF, Artes PH, O'Leary N, et al. Peripapillary choroidal thickness in healthy controls and patients with focal, diffuse, and sclerotic glaucomatous optic disc damage. *Arch Ophthalmol*. 2012;130:980–986.
42. Gupta P, Cheung CY, Baskaran M, et al. Relationship between peripapillary choroid and retinal nerve fiber layer thickness in a population-based sample of nonglaucomatous eyes. *Am J Ophthalmol*. 2016;161:4–11.e12.
43. Lamparter J, Schulze A, Riedel J, et al. Peripapillary choroidal thickness and choroidal area in glaucoma, ocular hypertension and healthy subjects by SD-OCT. *Klin Monbl Augenheilkd*. 2015;232:390–394.
44. Ho J, Branchini L, Regatieri C, Krishnan C, Fujimoto JG, Duker JS. Analysis of normal peripapillary choroidal thickness via spectral domain optical coherence tomography. *Ophthalmology*. 2011;118:2001–2007.
45. See JL, Nicolela MT, Chauhan BC. Rates of neuroretinal rim and peripapillary atrophy area change: a comparative study of glaucoma patients and normal controls. *Ophthalmology*. 2009;116:840–847.
46. Jonas JB, Fernandez MC, Sturmer J. Pattern of glaucomatous neuroretinal rim loss. *Ophthalmology*. 1993;100:63–68.
47. Strouthidis NG, Yang H, Reynaud JF, et al. Comparison of clinical and spectral domain optical coherence tomography optic disc margin anatomy. *Invest Ophthalmol Vis Sci*. 2009;50:4709–4718.
48. Strouthidis NG, Grimm J, Williams GA, Cull GA, Wilson DJ, Burgoyne CF. A comparison of optic nerve head morphology viewed by spectral domain optical coherence tomography and by serial histology. *Invest Ophthalmol Vis Sci*. 2010;51:1464–1474.
49. Burgoyne CF, Downs JC. Premise and prediction-how optic nerve head biomechanics underlies the susceptibility and clinical behavior of the aged optic nerve head. *J Glaucoma*. 2008;17:318–328.
50. Chauhan BC, O'Leary N, Almobarak FA, et al. Enhanced detection of open-angle glaucoma with an anatomically accurate optical coherence tomography-derived neuroretinal rim parameter. *Ophthalmology*. 2013;120:535–543.
51. Wu Z, Thenappan A, Weng DSD, Ritch R, Hood DC. Detecting glaucomatous progression with a region-of-interest approach on optical coherence tomography: a signal-to-noise evaluation. *Trans Vis Sci Tech*. 2018;7(1):19.
52. Silvio Di S, Luca A, Federico Di S, Hilary C, Marco C, Gian Luca S. Diagnostic capability of optic nerve head rim width and retinal nerve fiber thickness in open-angle glaucoma. *Eur J Ophthalmol*. 2018;28:459–464.
53. Toshev AP, Lamparter J, Pfeiffer N, Hoffmann EM. Bruch's membrane opening-minimum rim width assessment with spectral-domain optical coherence tomography performs better than confocal scanning laser ophthalmoscopy in discriminating early glaucoma patients from control subjects. *J Glaucoma*. 2017;26:27–33.
54. Tatham AJ, Medeiros FA. Detecting structural progression in glaucoma with optical coherence tomography. *Ophthalmology*. 2017;124:S57–S65.
55. Jonas JB, Jonas SB, Jonas RA, et al. Parapapillary atrophy: histological gamma zone and delta zone. *PLoS One* 2012;7:e47237.
56. Dai Y, Jonas JB, Huang H, Wang M, Sun X. Microstructure of parapapillary atrophy: beta zone and gamma zone. *Invest Ophthalmol Vis Sci*. 2013;54:2013–2018.
57. Miki A, Ikuno Y, Weinreb RN, et al. Measurements of the parapapillary atrophy zones in en face optical coherence tomography images. *PLoS One*. 2017;12:e0175347.
58. Chauhan BC, Burgoyne CF. From clinical examination of the optic disc to clinical assessment of the optic nerve head: a paradigm change. *Am J Ophthalmol*. 2013;156:218–227.e2.

Investigative Ophthalmology & Visual Science